World Academy of Science, Engineering and Technology
International Journal of Mechanical and Mechatronics Engineering
Vol:16, No:9, 2022

Numerical and Experimental Investigation of Airflow inside a Car Cabin

Mokhtar Djeddou, Amine Mehel, Georges Fokoua, Anne Tanière, Patrick Chevrier

***Abstract*—**Commuters' exposure to air pollution, particularly to particle matter inside vehicles, is a significant health issue. Assessing particle concentrations and characterizing their distribution is an important first step in understanding and proposing solutions to improve car cabin air quality. It is known that particle dynamics is intimately driven by particle-turbulence interactions. In order to analyze and model pollutants distribution inside car cabins, it is crucial to examine first the single-phase flow topology and its associated turbulence characteristics. Within this context, Computational Fluid Dynamics (CFD) simulations were conducted to model airflow inside a full-scale car cabin using Reynolds Averaged Navier-Stokes (RANS) approach combined with the first order Realizable k-ε model to close the RANS equations. To assess the numerical model, a campaign of velocity field measurements at different locations in the front and back of the car cabin has been carried out using hot-wire anemometry technique. Comparison between numerical and experimental results shows a good agreement of velocity profiles. Additionally, visualization of streamlines shows the formation of jet flow developing out of the dashboard air vents and the formation of large vortex structures, particularly between the front and back-seat compartments. These vortical structures could play a key role in the accumulation and clustering of particles in a turbulent flow.

***Keywords*—**Car cabin, CFD, hot-wire anemometry, vortical flow.

I. Introduction

AIR pollution inside car cabins is a major health issue. Commuters' exposure to particle matter raises serious health concerns as they contribute among other things to the risk of developing cardiovascular and respiratory diseases, as well as lung cancer [1]. The size of the particles has been directly related to their hazardousness. Small particles of concern include coarse inhalable particles with a diameter of 2.5 µm to 10 µm, fine particles with a diameter between 0.1 µm and 2.5 µm [2], and ultrafine particles with a diameter below 0.1 µm.

Particle dynamics is known to be highly influenced by their interaction with turbulent eddies of the carrier flow [3]. Therefore, attention must be devoted to modeling accurately airflow inside car cabins.

Airflow inside car cabins had been investigated in previous studies particularly in the context of thermal comfort [4]-[7]. The common feature between these studies is the use of a simplified geometry of the interior cabin which may not reflect the real complex car-cabin geometries.

A real full-scale car cabin was employed in [8] to validate a CFD model by comparing velocity distribution in the jet flow area with experimental results obtained by a PIV (Particle Image Velocimetry) technique. This study was limited only to a jet flow region which does not represent a complete validation of a numerical model.

The purpose of the research reported here was to evaluate a CFD model of airflow inside a full-scale car cabin by comparing velocity profiles with measurements results obtained using hot-wire anemometry technique. This latter allows covering different positions inside the car cabin with high temporal resolution and thus to have a more complete characterization of the flow topology inside a real car cabin.

M. Djeddou is with LEMTA - University of Lorraine, 54500 Vandœuvre-lès-Nancy France (e-mail: mokhtar.djeddou@univ-lorraine.fr).

II. Experimental Setup

The campaign of airflow velocity measurement was conducted using hot-wire anemometry technique inside an SUV-type car cabin as illustrated in Fig. 1. An ISEL linear guide rail system was installed inside the car cabin allowing an automatic transversal displacement in the y-axis. To cover different positions in the vertical z-axis, the hotwire probe support system is manually moved and positioned. Data were acquired every 2 cm in the y-axis at the frequency of 100 kHz and the length of each individual data set was 2 x 10^6 samples (or 20 s).

First, velocity profiles measurement was performed without ventilation to estimate vibration signal as the car engine is turned on. Then, ventilation is activated, and each velocity profile measurement was repeated at least two times to deal with results' reproducibility. Measurement error estimation includes velocity variation due to the vibration and the mean deviation of the results between the repeated profiles.

Fig. 1 Positioning setup

III. Mathematical Model

CFD simulations were achieved by resolving the steady

incompressible Navier-Stokes equations using the Reynolds-averaged approach RANS combined to the turbulence first order Realizable k-ε model [9] to close the Reynolds stress tensor.

The momentum equation and the velocity field divergence-free condition are defined as:

$$\bar{u}_j \frac{\partial}{\partial x_j}(\rho \bar{u}_i) = -\frac{\partial \bar{p}}{\partial x_i} + \mu \frac{\partial^2 \bar{u}_i}{\partial x_j^2} + \frac{\partial}{\partial x_j}\left(-\rho \overline{u_i' u_j'}\right) \quad (1)$$

$$\frac{\partial \bar{u}_i}{\partial x_i} = 0 \quad (2)$$

where ρ: density; $\bar{u}_i$: mean velocity components; u_i': fluctuating velocity components; $\bar{p}$: mean pressure; μ: dynamic viscosity.

The Reynolds stress tensor is modeled using the Boussinesq hypothesis to relate the Reynolds stresses to the mean velocity gradients:

$$-\rho \overline{u_i' u_j'} = 2\mu_t S_{ij} - \frac{2}{3}(\rho k)\delta_{ij} \quad (3)$$

where μ_t: turbulent viscosity; $S_{ij} = \frac{1}{2}\left(\frac{\partial \bar{u}_i}{\partial x_j} + \frac{\partial \bar{u}_j}{\partial x_i}\right)$: mean strain rate tensor; $k = \frac{1}{2}\overline{u_i' u_i'}$: turbulent kinetic energy per unit mass; δ_{ij}: the Kronecker delta.

With this approach, modeling Reynolds stresses involves calculating the turbulent viscosity μ_t as an isotropic scalar quantity. This coefficient is obtained by solving two additional transport equations for the turbulence kinetic energy k and the turbulence dissipation rate ε.

$$\mu_t = \rho C_\mu \frac{k^2}{\varepsilon} \quad (4)$$

In the Realizable k-ε formulation, the transport equations for k and ε are expressed as follows [10]:

$$\bar{u}_j \frac{\partial}{\partial x_j}(\rho k) = \frac{\partial}{\partial x_j}\left[\left(\mu + \frac{\mu_t}{\sigma_k}\right)\frac{\partial k}{\partial x_j}\right] + \mu_t S^2 - \rho\varepsilon \quad (5)$$

$$\bar{u}_j \frac{\partial}{\partial x_j}(\rho \varepsilon) = \frac{\partial}{\partial x_j}\left[\left(\mu + \frac{\mu_t}{\sigma_\varepsilon}\right)\frac{\partial \varepsilon}{\partial x_j}\right] + \rho C_1 S\varepsilon - \rho C_2 \frac{\varepsilon^2}{k + \sqrt{\mu\varepsilon/\rho}} \quad (6)$$

where:

$$C_1 = \max\left[0.43, \frac{\eta}{\eta+5}\right], \eta = S\frac{k}{\varepsilon}, S = \sqrt{2S_{ij}S_{ij}}$$

In these equations, σ_k and σ_ε are the turbulent Prandtl numbers for k and ε respectively equal to 1 and 1.2, and C_2 is a constant equal to 1.9.

In the near-wall region, the mean velocity field and the turbulence quantities are significantly affected by the presence of walls. The mean velocity field must satisfy the no-slip condition and the velocity profile must therefore vanish at the wall, which results in significant gradients for the flow variables. Another important feature is the increase in turbulent kinetic energy production due to large velocity gradients near the wall.

To resolve accurately airflow in this viscosity-affected region, the enhanced wall treatment model (EWT) is employed. This model is based on the two layers approach. The whole domain is subdivided into two distinct regions depending on the turbulent Reynolds number, Re_y, based on the wall-normal distance, y, and defined as:

$$Re_y = \frac{\rho y \sqrt{k}}{\mu}$$

In the fully turbulent region $(Re_y > 200)$, the k-ε model is employed. While in the viscosity-affected near-wall region $(Re_y < 200)$, the turbulence model is modified to enable the viscosity-affected region to be resolved with a mesh all the way to the wall, including the viscous sublayer [10].

IV. Simulation Setup

A. Boundary Conditions

CFD simulations were completed using ANSYS Fluent 19.2 solver [10]. The fluid volume of a full-scale car's interior has been reconstructed based on the cabin CAD as illustrated in Fig. 2. The HVAC system had been modeled from its outlets, i.e., the last parts of the air hoses and the air vents. The cabin inlet boundaries for the inflow are set upstream the air vents and the outlets boundaries are in the car trunk compartment (blue surfaces in Fig. 2) and set as atmospheric pressure. A mean velocity of $4.2\ m/s$ was imposed on the air-vent inlets corresponding to a Reynolds number ranging from $2.6\ 10^5$ to $3.2\ 10^5$ based on the air-vent-inlet mean velocity and equivalent diameter.

B. Mesh

A volume mesh of about ~10 million polyhedral cells was generated using ANSYS Fluent meshing 19.2. Five boundary layers were applied to all surface walls.

Polyhedral mesh combines the advantages of hexahedrons (low numerical diffusion and lower cell count) and tetrahedrons (rapid generation and more adapted to complex geometry). Each individual cell has many neighbors, so gradients are well approximated. Numerical diffusion is reduced due to mass exchange over numerous faces which leads to a more accurate solution. Polyhedral cells present also the advantage of being less sensitive to stretching than tetrahedrons, which results in a better mesh quality and thus a better numerical stability of the model [11].

The mesh quality is assessed by examining statistics of skewness, aspect ratio, and size change parameters.

Skewness determines how close to ideal (that is, equilateral or equiangular) a face or cell is [10]. The maximum cell skewness reported is approximately 0.85 and most cells have a skewness value below 0.2 (Fig. 5). This indicates a good mesh quality.

The aspect ratio of a cell is the ratio of the longest edge length to the shortest edge length [10]. The reported average value of the cell aspect ratio is 5.28 with the main peak at 1.3. These values are reasonably acceptable considering the geometry complexity.

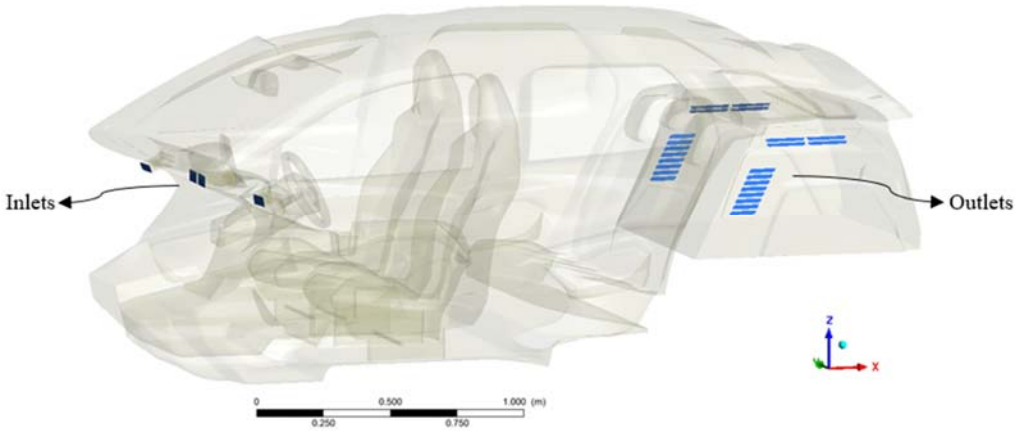

Fig. 2 Car cabin's fluid volume

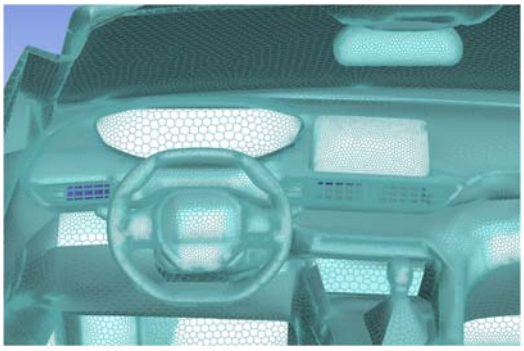

Fig. 3 Surface mesh (zoom on the dashboard)

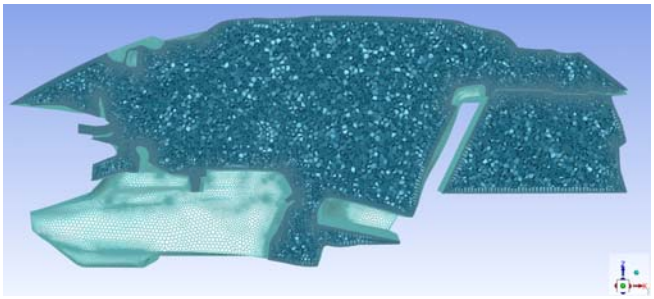

Fig. 4 Volume mesh (central xz-plane)

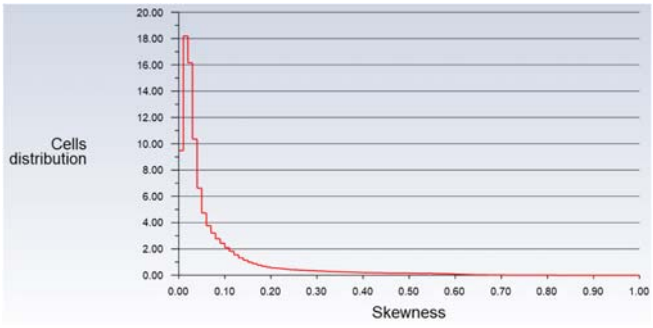

Fig. 5 Mesh quality (Skewness)

Cell size change is the ratio of the volume of a cell in the geometry to the volume of each neighboring cell [10]. Fig. 7 shows that cells are distributed around a reported average value of 2.26, which indicates no large jump in cell size.

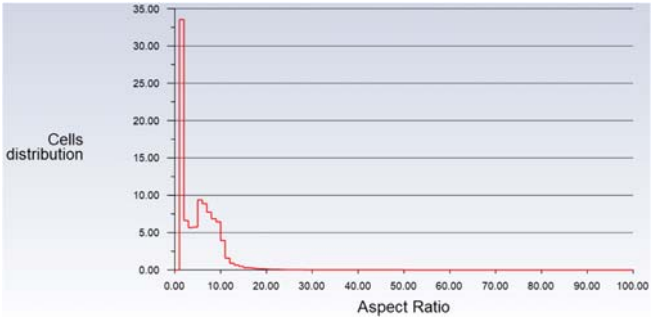

Fig. 6 Mesh quality (aspect ratio)

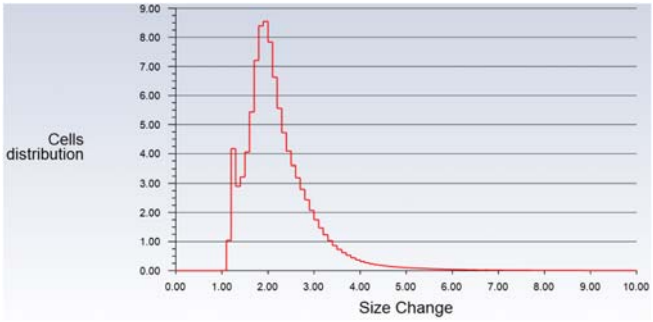

Fig. 7 Mesh quality (Size change)

1) Post-processing

We compared simulation results of streamwise velocity profiles at different positions with experimental results. We limit ourselves to presenting only two planes, one in the front seat compartment of the car, denominated “plane 1”, and the second plane in the back-seat compartment, denominated “plane 2”. Compared profiles are designated by their plane number (1 or 2) and their vertical position is illustrated in Fig. 8.

The y-axis origin corresponds to the mid-width central plane of the car. Profiles are spaced by 4.25 cm in the vertical z-axis. The highest horizontal profiles “P2H7” and “P2H8” in Fig. 8 are shorter than the others due to the curved car roof on the sides.

V. Results and Discussion

A. Comparison between Numerical and Experimental Results

Figs. 9 and 10 show a comparison between numerical and experimental profiles of the mean x-component velocity normalized by the inlet mean velocity ($U_0 = 4.2\ m/s$) in plane 1 and plane 2.

In Fig. 9 CFD simulation results are essentially in good agreement with the experiment for all compared profiles. However, some differences can be observed around positions y = 0 but generally, the CFD model reproduces reasonably well the measured velocity profiles.

Maxima in the velocity profiles indicate the jets flow issued from the central air vents. We notice that the value of the peaks of the central jets are not the same for all air vents. This asymmetry is due to the inclined geometry of the dashboard air vents which are slightly oriented towards the driver's seat. This asymmetry has already been observed in another study of jet flow inside a car cabin [8]. On the other hand, velocity profiles in the back-seat plane (Fig. 10) present some discrepancies between simulations and measurements which can be explained by the complex interaction between airflow and in-cabin equipment (such as seats, head rests, etc.). Despite these relative differences, numerical velocity profiles show the same trend compared to the experimental profiles.

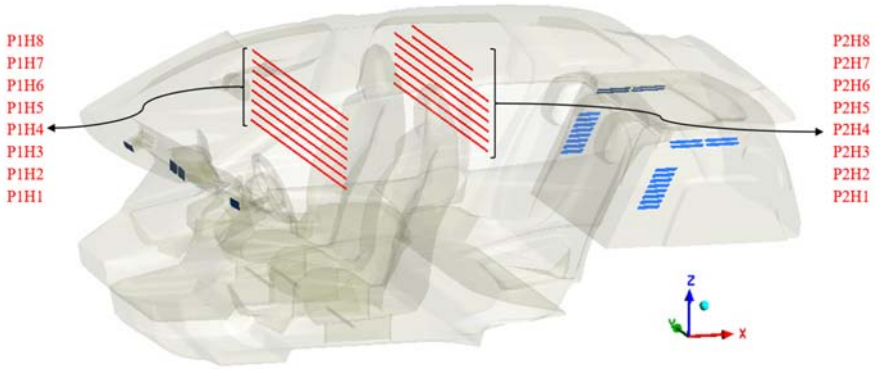

Fig. 8 Compared profiles localization

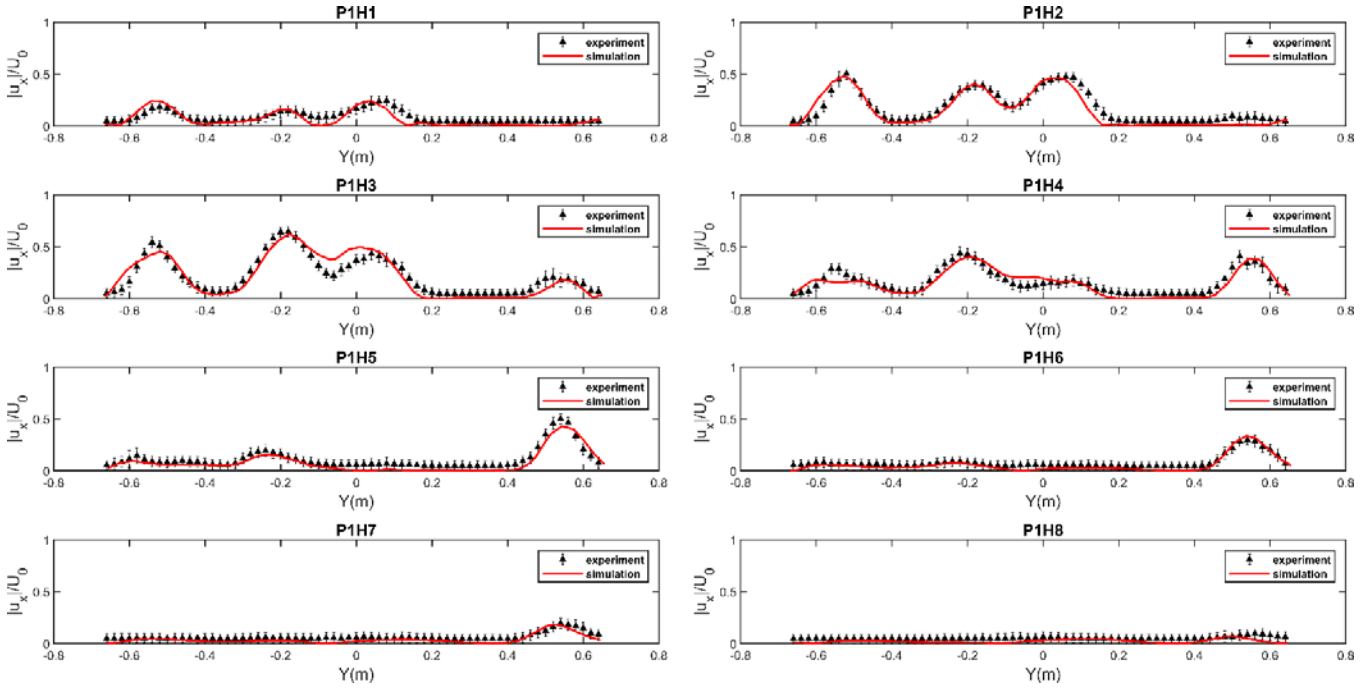

Fig. 9 Comparison between numerical and experimental normalized mean x-component velocity profiles (plane 1)

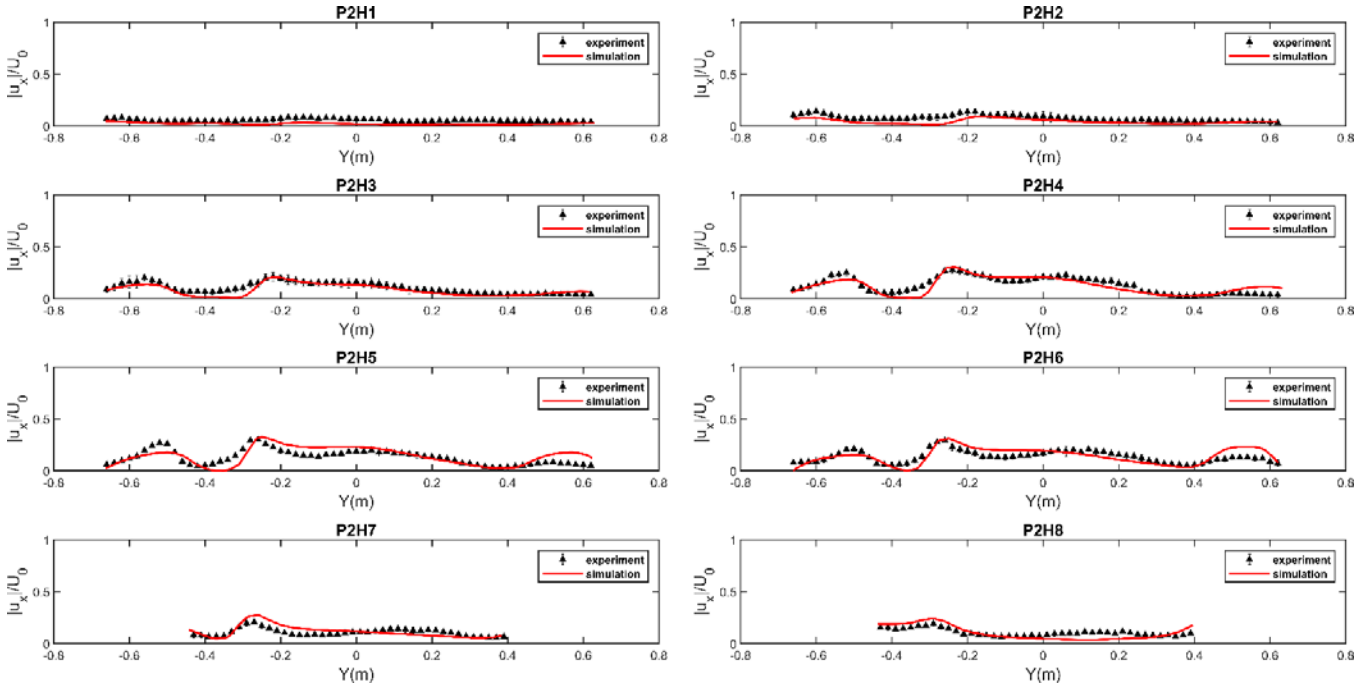

Fig. 10 Comparison between numerical and experimental normalized mean x-component velocity profiles (plane 2)

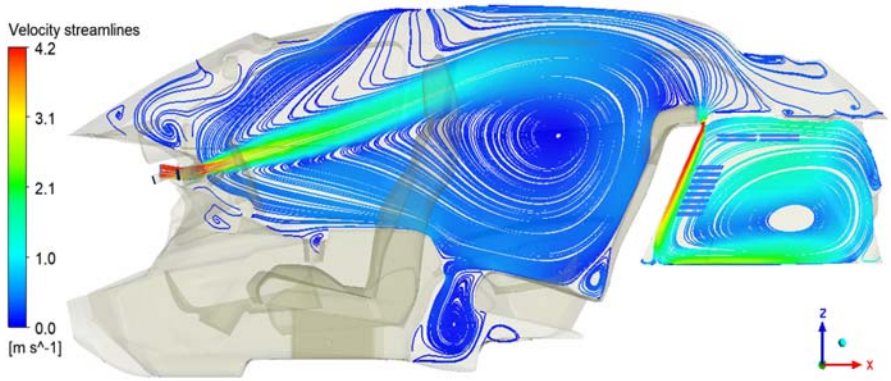

Fig. 11 Streamlines in the car streamwise central plane

B. Global in-Cabin Airflow Topology

Visualization of streamlines on the central plane of the car cabin (Fig. 11) shows the formation of a jet flow developing out of the dashboard air vent and expanding to the back-seat compartment. This results in a large vortex structure occupying the whole back-seat compartment volume.

Due to the existing tiny gap on the car shelf and the position of the outlet boundaries, airflow enters the trunk compartment to form a large swirl structure confined in the limited volume of the trunk. Other vortical structures appear also, for example, at the feet level, and it is expected that it influences particles dynamics.

VI. Conclusion

Airflow inside an SUV-type car cabin was investigated using CFD simulation, based on the RANS approach combined with the Realizable k-ε model. The velocity field measurement at different positions using a hotwire anemometry technique has been also achieved.

Comparison between numerical results of the normalized mean x-component velocity profiles with experimental results shows a good consistency of the CFD model. Numerical and experimental velocity profiles are in good agreement.

Visualization of airflow streamlines shows a jet flow developing out the dashboard air vents and the formation of several vortical structures as the large vortex structure in the back-seat compartment. The next step is the simulation of particles dynamics, infiltrating from outside, in the car cabin in conjunction with the airflow topology. The final objective is to bring knowledge for an optimized solution to reduce pollution in such confined spaces.

References

[1] World Health Organization (WHO), "Health effects of particulate matter. Policy implications for countries in eastern Europe, Caucasus and central Asia," Copenhagen, 2013.

[2] K.-H. Kim, E. Kabir et S. Kabir, «A review on the human health impact

of airborne particulate matter,» Environment International, 2015.
[3] L. I. Zaichik, V. M. Alipchenkov and E. G. Sinaiski, Particles in Turbulent Flows, Weinheim: WILEY-VCH Verlag GmbH & Co. KGaA, 2008.
[4] Y. Ishihara, J. Hara, H. Sakamoto, K. Kamemoto and H. Okamoto, "Determination of Flow Velocity Distribution in a Vehicle Interior Using a Visualization and Computation Techniques," SAE Technical Paper, 1991.
[5] A. Piovano, L. Lorefice and O. Scantamburlo, "Modelling of Car Cabin Thermal Behaviour during Cool Down, Using an Advanced CFD/Thermal Approach," SAE Technical Paper, 2016.
[6] P. Danca, F. Bode, I. Nastase and A. Meslem, "On the possibility of CFD modeling of the indoor environment in a vehicle," Energy Procedia, 2016.
[7] T.-B. Chang, J.-J. Sheu, J.-W. Huang and Y.-S. Lin, "Development of a CFD model for simulating vehicle cabin indoor air quality," Transportation Research Part D, 2018.
[8] S. Ullrich, R. Buder, N. Boughanmi, C. Friebe and C. Wagner, "Numerical Study of the Airflow Distribution in a Passenger Car Cabin Validated with PIV," in New Results in Numerical and Experimental Fluid Mechanics XII, 2020.
[9] T.-H. Shih, W. W. Liou, A. Shabbir, Z. Yang and J. Zhu, "A New k-ε Eddy Viscosity Model for High Reynolds Number Turbulent Flows - Model Development and Validation," Computers & Fluids, 1994.
[10] ANSYS Inc, ANSYS Fluent Theory Guide, Canonsburg, 2019.
[11] M. Sosnowski, J. Krzywanski, K. Grabowska and R. and Gnatowska, "Polyhedral meshing in numerical analysis of conjugate heat transfer," in European Physical Journal Web of Conferences, 2018.